Shear Viscosities and Normal Stress Differences of Rigid Liquid-Crystalline Polymers

Yu-Guo Tao, W. K. den Otter, and W. J. Briels*

Computational Biophysics, Faculty of Science and Technology, University of Twente, P.O. Box 217, 7500 AE Enschede, The Netherlands

Received March 20, 2006; Revised Manuscript Received June 2, 2006

ABSTRACT: Shear viscosities as well as first and second normal stress differences of solutions of rigid spherocylindrical colloids are investigated by Brownian dynamics simulations for aspect ratios L/D in a range from 25 to 60 and scaled volume fractions $L\varphi/D$ from 0.5 to 4.5. Shear thinning behavior is observed in all cases. In the isotropic phase, the calculated viscosities at low volume fractions are in agreement with predictions by Dhont and Briels, while over a larger range of shear rates they are described by the Hess equation. The self-rotational diffusion coefficients obtained from the flow curves agree very well with those calculated by traditional methods. In the nematic phase, the inflection point of the flow curve is associated with the critical shear rate at which the orientational director changes its motion from kayaking to wagging. The first normal stress difference N_1 in the nematic solution is positive at low and high shear rates but negative at moderate rates, which is rather distinct from the monotone behavior shown by isotropic solutions. The simulated second normal stress difference N_2 is found much smaller in amplitude than N_1 and always opposite in sign. Our findings qualitatively confirm existing theoretical predictions and experimental measurements. A newly developed event-driven Brownian dynamics algorithm, in which the excluded-volume interactions between particles are incorporated as collisions instead of as repulsive potentials, has made these simulations feasible.

1. Introduction

Suspensions of nematic rodlike colloids or liquid crystalline polymers (LCPs) in shear flow exhibit unusual rheological behaviors, such as pronounced oscillations of the stress against time or a negative first normal stress difference at intermediate shear rates. Because of this complex dynamics, as compared to conventional polymer liquids, concentrated lyotropic LCPs aroused much scientific interest both in theoretical predictions[1−27] and in experimental observations.[28−41] Hess[1] and Doi[2] suggested a molecular theory of rodlike LCPs in shear flow. The Doi−Hess theory has been solved numerically by restricting it to two dimensions[9] or by expanding the orientational distribution function in spherical harmonics,[12,15] or by one-particle Brownian dynamics in a mean-field potential.[27] It was found that the director, i.e., the average direction of the rods, exhibits tumbling, kayaking, wagging, flow-aligning, or log-rolling types of motion, depending on the applied shear rates. The theoretical investigations revealed that all peculiar behaviors mentioned above are to be attributed to the periodic oscillation of the director.

Besides theoretical and experimental investigations, computer simulation becomes an increasingly valuable supplement in the quest to understand complex LCPs. Unfortunately, the previous computational studies on the rheology of rigid rods only focused on isotropic solutions[42,43] or rods with small aspect ratios.[44] To study suspensions of rigid long and thin rods in shear flow, we[45−47] recently developed an event-driven Brownian dynamics simulation algorithm in which excluded-volume interactions between rods are taken into account but hydrodynamic interactions are considered unimportant and negligible. This algorithm has its inherent novelty in preventing the overlaps between interacting rods by carefully controlling the collisions in stead of by applying a repulsive potential. By this algorithm, the collective periodic orientational motions of the directors of nematic solutions of rigid rods with large shape anisotropy are clearly described for the first time.[45,47] As a supplement of the previous work, we continue our investigations with the rheological properties, i.e., viscosities and normal stress differences, of rigid Brownian rods in shear flow.

This paper is organized as follows: In section 2 we briefly discuss the microscopic theory for the viscoelastic behavior of suspensions of rigid rods with excluded volume interactions. In sections 3.1 and 3.2 we investigate the shear rate dependence of the viscosities of rodlike colloids in isotropic and nematic phases, respectively, while the calculated first and second normal stress differences are presented in section 3.3. Finally, we summarize our conclusions in section 4. The algorithm of the event-driven Brownian dynamics simulation is omitted in the present paper, since it has already been discussed in our previous publications.[45−47]

2. Theory

In this section we briefly comment on the expression that we have used to calculate stresses from our simulation data. To motivate our choice, we start with the one-particle Smoluchowski equation[20]

$$\frac{\partial}{\partial t}P(\hat{\mathbf{u}},t) = D_r\hat{\mathscr{R}}\cdot\left\{\hat{\mathscr{R}}\,P(\hat{\mathbf{u}},t) - \frac{1}{k_BT}P(\hat{\mathbf{u}},t)\,\bar{\mathbf{T}}(\hat{\mathbf{u}},t)\right\} - \hat{\mathscr{R}}\cdot P(\hat{\mathbf{u}},t)\hat{\mathbf{u}}\times(\boldsymbol{\Gamma}\cdot\hat{\mathbf{u}}) \quad (1)$$

describing the time evolution of the one-particle orientational probability distribution $P(\hat{\mathbf{u}},t)$ of a collection of rods at time t with unit vectors $\hat{\mathbf{u}}$ along their long axes. The rotational operator $\hat{\mathscr{R}}$ is defined as $\hat{\mathscr{R}} \equiv \hat{\mathbf{u}} \times (\partial/\partial\hat{\mathbf{u}})$ and plays a role very similar to that of the gradient operator ∇_r in the description of translational diffusion. D_r is the rotational diffusion coefficient of a single rod

* Corresponding author. E-mail: w.j.briels@utwente.nl.

10.1021/ma060622q CCC: $33.50
Published on Web 07/20/2006

$$D_r = \frac{3k_BT\ln(L/D)}{\pi\eta_s L^3} \tag{2}$$

with η_s the viscosity of the solvent. k_B is Boltzmann's constant and T the temperature. Γ is the velocity gradient tensor, related to the flow velocity $\mathbf{V}$ at position $\mathbf{r}$ by $\mathbf{V} = \Gamma\cdot\mathbf{r}$; in this work $\Gamma = \dot\gamma\hat{\mathbf{e}}_x\hat{\mathbf{e}}_y$ with $\dot\gamma$ the shear rate and $\hat{\mathbf{e}}_\alpha$ a unit vector in the α-direction. The average torque acting on the central rod $\bar{\mathbf{T}}(\hat{\mathbf{u}},t)$ in eq 1 is expressed as

$$\bar{\mathbf{T}}(\hat{\mathbf{u}},t) = -\bar\rho\int d\mathbf{r}' \oint d\mathbf{u}'\, P(\hat{\mathbf{u}}', t)\, g(\mathbf{r}-\mathbf{r}', \hat{\mathbf{u}}, \hat{\mathbf{u}}', t)\times \hat{\mathscr{R}}\, V(\mathbf{r}-\mathbf{r}', \hat{\mathbf{u}}, \hat{\mathbf{u}}') \tag{3}$$

where $\bar\rho$ is the number density of rods and $V(\mathbf{r}-\mathbf{r}', \hat{\mathbf{u}}, \hat{\mathbf{u}}')$ is the pair-interaction potential for two rods with orientations $\hat{\mathbf{u}}$ and $\hat{\mathbf{u}}'$ and center−center separation $\mathbf{r}-\mathbf{r}'$; similarly, $g(\mathbf{r}-\mathbf{r}', \hat{\mathbf{u}}, \hat{\mathbf{u}}', t)$ is the pair correlation function for the two rods mentioned above at time t. The main approximation made in deriving eq 1 was to neglect hydrodynamic interactions between the rods. For analytical purposes, we now neglect the time dependence of the pair correlation function and approximate it by its equilibrium value for very long rods

$$g(\mathbf{r}-\mathbf{r}'\,\hat{\mathbf{u}}, \hat{\mathbf{u}}', t) = \exp\left\{-\frac{1}{k_BT}V(\mathbf{r}-\mathbf{r}'\,\hat{\mathbf{u}}, \hat{\mathbf{u}}')\right\} \tag{4}$$

Making one more approximation when expanding $|\hat{\mathbf{u}}\times\hat{\mathbf{u}}'|$ up to second order in orthogonal polyadic products of $\hat{\mathbf{u}}$'s,[46] we may calculate the equation of motion of the order tensor $\mathbf{S} = \langle\hat{\mathbf{u}}\hat{\mathbf{u}}\rangle$, with the brackets denoting an ensemble average, obtaining[20]

$$\frac{d}{dt}\mathbf{S} = -6D_r\left\{\mathbf{S} - \frac{1}{3}\hat{\mathbf{I}} + \frac{5}{4}\frac{L}{D}\varphi(\mathbf{S}^{(4)}:\mathbf{S} - \mathbf{S}\cdot\mathbf{S})\right\} + \dot\gamma\{\hat\Gamma\cdot\mathbf{S} + \mathbf{S}\cdot\hat\Gamma^T - 2\mathbf{S}^{(4)}:\hat{\mathbf{E}}\} \tag{5}$$

where $\hat{\mathbf{I}}$ is the unit tensor, $\hat\Gamma = \Gamma/\dot\gamma$, and $\hat{\mathbf{E}} = {}^1/_2[\hat\Gamma + \hat\Gamma^T]$, with the superscript "T" denoting a transposition. The volume fraction is defined as $\varphi = {}^1/_4\bar\rho\pi D^2L$. $\mathbf{S}^{(4)}$ is a fourth-order tensor defined by $\mathbf{S}^{(4)} = \langle\hat{\mathbf{u}}\hat{\mathbf{u}}\hat{\mathbf{u}}\hat{\mathbf{u}}\rangle$. In a previous paper,[48] we have argued that most probably the last two approximations mentioned above are the most severe in determining the quality of eq 5. It is important to notice that they are only used in calculating the term proportional to $L\varphi/D$. The extra factor of 5/4 in this term as compared to the corresponding term in ref 20 has been explained in our previous paper.[46]

The expression needed to calculate the deviatoric part Σ of the stress tensor has been derived by Dhont and Briels[20,21] and reads

$$\Sigma = 2\eta_s\dot\gamma\hat{\mathbf{E}} + 3\bar\rho k_BT\left\{\mathbf{S} - \frac{1}{3}\hat{\mathbf{I}} + \frac{5}{4}\frac{L}{D}\varphi(\mathbf{S}^{(4)}:\mathbf{S} - \mathbf{S}\cdot\mathbf{S}) + \frac{1}{6}\frac{\dot\gamma}{D_r}\left(\mathbf{S}^{(4)}:\hat{\mathbf{E}} - \frac{1}{3}\hat{\mathbf{I}}\mathbf{S}:\hat{\mathbf{E}}\right)\right\} \tag{6}$$

Also here the somewhat uncontrolled approximations concerning the pair correlation function are only used in a term proportional to $L\varphi/D$, which carries a factor of 5/4 for the same reason as the term proportional to $L\varphi/D$ in eq 5. Fortunately, apart from a constant factor, both terms proportional to $L\varphi/D$ are equal in eqs 5 and 6, and so we may eliminate the one in eq 6, obtaining[20]

$$\Sigma = 2\eta_s\dot\gamma\hat{\mathbf{E}} + \frac{2(L/D)^2}{3\ln(L/D)}\varphi\eta_s\dot\gamma\left\{\hat\Gamma\cdot\mathbf{S} + \mathbf{S}\cdot\hat\Gamma^T - \mathbf{S}^{(4)}:\hat{\mathbf{E}} - \frac{1}{3}\hat{\mathbf{I}}\mathbf{S}:\hat{\mathbf{E}} - \frac{1}{\dot\gamma}\frac{d\mathbf{S}}{dt}\right\} \tag{7}$$

This expression for Σ may be considered to be largely independent of any approximations concerning the pair correlation function. Obviously, it still suffers from the neglect of hydrodynamic interactions, which under some circumstances may be important. The term proportional to $d\mathbf{S}/dt$ in eq 7 will be ignored for the following reasons. In the isotropic state, i.e., at low volume fractions, the order tensor is constant, and consequently $d\mathbf{S}/dt$ has no contribution at all. In the nematic state at low shear rates, the order tensor varies periodically in time with constant period, meaning that $d\mathbf{S}/dt$ is nonzero. In the present work, however, we will calculate viscosities and normal stress differences averaged over integer numbers of oscillation periods, rendering zero the contributions of $d\mathbf{S}/dt$ to the final results. In the nematic state at very high shear rates, the order tensor becomes constant and $d\mathbf{S}/dt = 0$ again.

In our simulations, we impose a simple shear flow in the x-direction with gradient in the y-direction. The relative viscosity η^* averaged over time reads

$$\eta^* = \frac{\bar\Sigma_{xy}}{\dot\gamma\eta_s} = 1 + \frac{2(L/D)^2}{3\ln(L/D)}\varphi\left(\hat\Gamma\cdot\mathbf{S} + \mathbf{S}\cdot\hat\Gamma^T - \mathbf{S}^{(4)}:\hat{\mathbf{E}} - \frac{1}{3}\hat{\mathbf{I}}\mathbf{S}:\hat{\mathbf{E}}\right) \tag{8}$$

while first and second normal stress differences are calculated from their definitions:

$$N_1 \equiv \bar\Sigma_{xx} - \bar\Sigma_{yy} \tag{9}$$

$$N_2 \equiv \bar\Sigma_{yy} - \bar\Sigma_{zz} \tag{10}$$

The bars in $\bar\Sigma_{xy}$ denote a time averaging.

3. Results and Discussion

In this section, we describe our simulation results of stresses in solutions of rodlike colloids. First, we address shear viscosities of isotropic systems as a function of shear rate. Next, we discuss similar results for nematic phases and finally we study first and second normal stress differences in both isotropic and nematic phases in shear flow.

The simulated rigid rods are based on experimental data of the *fd* viruses.[49,50] These rodlike biopolymers, because of their monodispersity and well-characterized interparticle interactions, are considered to be among the best representatives of rigid rods for experimental purposes. For a recent review article, we refer the reader to Dogic and Fraden.[51] Our simulation boxes were cubic, and periodic boundary conditions were employed in both the velocity and vorticity direction, while the Lees−Edwards boundary conditions were used in the gradient direction.[52] Box volumes were chosen according to $V = c(\pi/4)(L/D)^{-1}L^3$ with $c = 500$ for $L/D \le 40$, $c = 750$ for $L/D = 50$, and $c = 1000$ for $L/D = 60$. By doing so, the edges of the boxes were always 2.5−3 times as large as the rod lengths. The number of rods N was obtained from $N = cL\varphi/D$ and ranged from 250 to 4500. The diameter was chosen to be 14.8 nm. Water was used as solvent, with viscosity $\eta_s = 10^{-3}$ Pa·s. The temperature was 300 K in all cases. The event-driven algorithm described previously[46] was used with a time step δt of 0.5 μs, which is at least 1 order of magnitude larger than that used in simulations[48] using semihard interactions between rods.

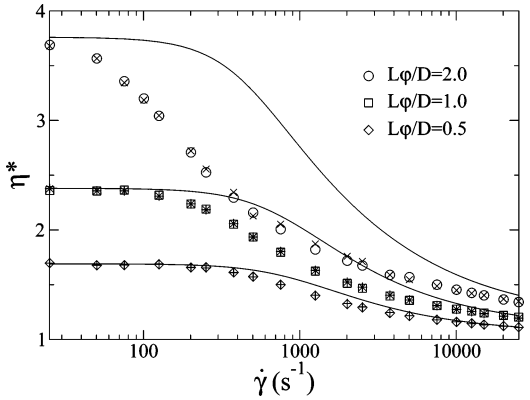

Figure 1. Relative viscosities of isotropic suspensions of rigid rods with aspect ratio $L/D = 25$ for three scaled volume fractions. Circles, squares, and diamonds represent the results for $L\varphi/D = 2.0$, 1.0, and 0.5, respectively, while crosses, stars, and pluses represent the corresponding η^* obtained by using the closure eq 11 on the basis of order tensors **S** from the simulations. Curves represent theoretical results predicted by Dhont and Briels.[20]

3.1. Shear Thinning of Isotropic Systems. In Figure 1 we have plotted the relative viscosities η^* as a function of shear rate for three isotropic systems consisting of rods with aspect ratio equal to 25. A clear shear thinning is observed in all cases. For comparison, we have included the results obtained by calculating $\mathbf{S}^{(4)}:\hat{\mathbf{E}}$ in eq 7 using the closure relation

$$\mathbf{S}^{(4)}:\hat{\mathbf{E}} \approx \frac{1}{5}\{\mathbf{S}\cdot\hat{\mathbf{E}} + \hat{\mathbf{E}}\cdot\mathbf{S} - \mathbf{S}\cdot\mathbf{S}\cdot\hat{\mathbf{E}} - \hat{\mathbf{E}}\cdot\mathbf{S}\cdot\mathbf{S} + 2\mathbf{S}\cdot\hat{\mathbf{E}}\cdot\mathbf{S} + 3\mathbf{SS}:\hat{\mathbf{E}}\} \quad (11)$$

on the basis of the simulated orientational order tensor **S**. The viscosities calculated by using the closure eq 11 are seen to be within ≈3% of the exact values in the case of isotropic suspensions. Apparently, the above closure is very accurate, in agreement with previous findings of ours.[48] Also shown in Figure 1 are viscosities calculated by means of a theory by Dhont and Briels,[20] using the approximate pair correlation function of eq 4. In the case of $L\varphi/D = 0.5$ the agreement is very good, and the neglect of dynamic correlations is apparently unimportant. This holds true to a lesser extent when $L\varphi/D = 1$. For $L\varphi/D = 2$ the agreement is limited to the lowest shear rates, which was to be expected since this volume fraction is rather close to the isotropic−nematic phase transition where a good description of pair correlations becomes increasingly important.

Some 20 years ago, Hess has suggested that these viscosities may be described by[53,54]

$$\eta^* = \eta^*_\infty + \frac{\eta^*_0 - \eta^*_\infty}{1 + (\dot\gamma\tau_r)^2} \quad (12)$$

where η^*_0 and η^*_∞ are the values at zero shear rate and very large shear rates, respectively. τ_r is a characteristic time given by $\tau_r = 1/6D_r(\varphi)$. This latter expression has been tested experimentally by Graf et al.[36] on isotropic systems of *fd* viruses. By fitting their measured viscosities with the Hess equation, they found $D_r(\varphi)$ in good agreement with self-rotational diffusion coefficients obtained from electric or magnetic birefringence experiments.[55−57] We have made similar fits and present the $D_r(\varphi)$ obtained this way in Figure 2, together with those obtained by calculating $D_r(\varphi)$ using

$$\langle\hat{\mathbf{u}}(t)\cdot\hat{\mathbf{u}}(0)\rangle = \exp\{-2D_r(\varphi)t\} \quad (13)$$

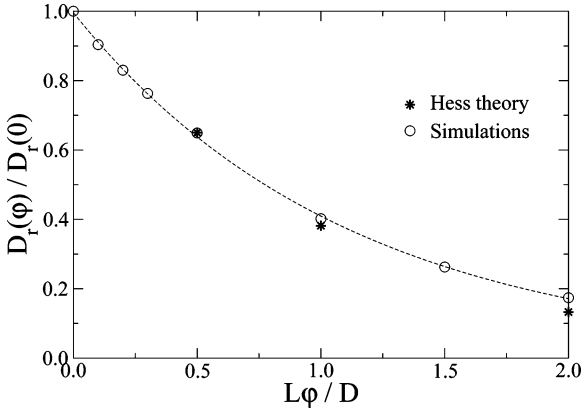

Figure 2. Self-rotational diffusion coefficients of rods with $L/D = 25$ in isotropic suspensions as a function of the scaled volume fraction. Circles denote the traditional measurements by using the Debye expression, eq 13, while stars are calculated from the viscosity by the Hess theory, eq 12.

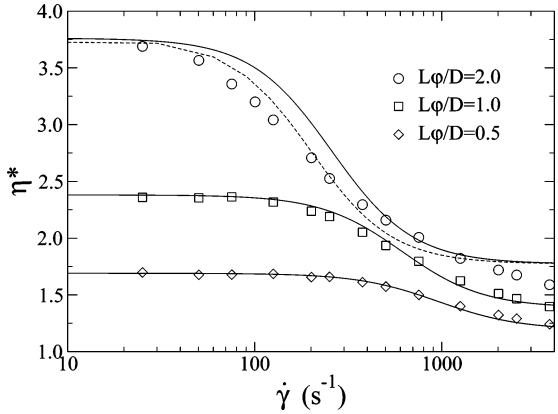

Figure 3. Relative viscosities of isotropic suspensions of rigid rods with $L/D = 25$ as a function of shear rate. Drawn lines show the results of eq 14 with $D_r(\varphi)$ calculated from the Debye expression, eq 13, while the dashed curve is a three-parameter fit with the Hess theory, eq 12.

It is seen that both methods yield results in very good agreement with each other.

In their review paper,[20] Dhont and Briels apply a perturbation theory to calculate viscosities of isotropic suspensions at low shear rates and low volume fractions. By expanding the Hess equation to the same order and comparing both expressions, η^*_0 and η^*_∞ may be calculated. Using the results in the Hess equation, we obtain

$$\eta^* = \left(1 + \alpha\frac{L}{D}\varphi\right) - \frac{18}{25}\frac{1}{1 + \left(\frac{6D_r(\varphi)}{\dot\gamma}\right)^2}\alpha\frac{L}{D}\varphi \quad (14)$$

where the coefficient α is given by

$$\alpha = \frac{8}{45}\frac{L/D}{\ln(L/D)} \quad (15)$$

In Figure 3 we compare viscosities obtained with this equation with those calculated from our simulation results. It is seen that for the lowest two volume fractions the results agree remarkably well. For $L\varphi/D = 2.0$ the agreement is less perfect, and in this case a fit with the Hess equation using η^*_0, η^*_∞, and τ_r as adjustable parameters performed slightly better, as indicated by the dashed line.

3.2. Shear Thinning of Nematic Systems. In this subsection we describe our results of calculating shear viscosities of nematic

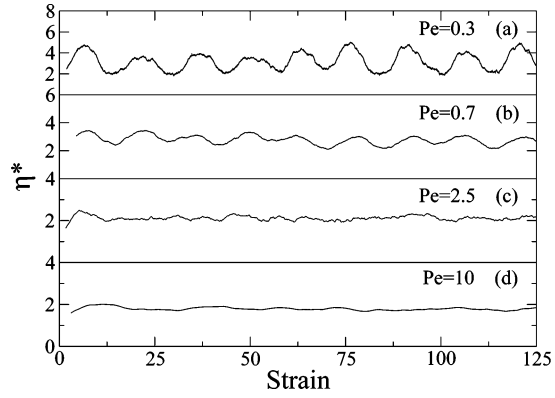

Figure 4. Relative viscosities η^*, calculated by eq 7 including the d**S**/dt term, as a function of strain. In panels a−d, four different shear rates are employed with the corresponding rotational Peclet numbers $Pe_r = 0.3$, 0.7, 2.5, and 10.0, respectively. A running average of d**S**/dt is used for each panel to reduce the noise produced by the numerical differentiation of **S**.

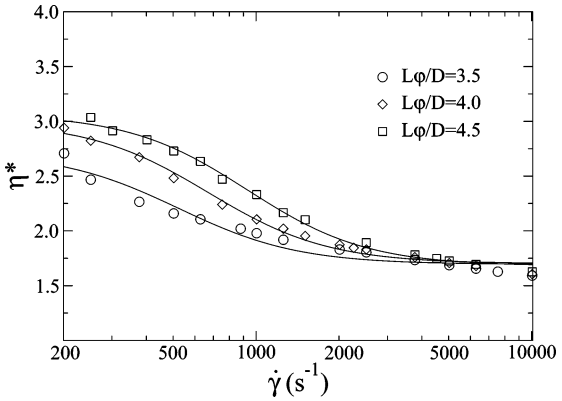

Figure 5. Relative viscosities of nematic suspensions of rigid rods with aspect ratio $L/D = 25$ at three scaled volume fractions of 3.5, 4.0, and 4.5, respectively.

systems. First, in Figure 4 we plot the relative viscosity as a function of strain for a nematic system of rods with aspect ratio equal to 25 and scaled volume fraction $L\varphi/D = 3.5$ for four different rotational Peclet numbers, $Pe_r = \dot{\gamma}/D_r$. The viscosities $\eta^*(t) = \Sigma_{xy}(t)/\dot{\gamma}\eta_s$ in this plot are not time averaged and are calculated using eq 7, including the term proportional to d**S**/dt. Similar calculations, neglecting the term proportional to d**S**/dt, reveal that this term smooths the results a bit but has no influence on the time-averaged results that we are interested in. In panels a and b, the viscosity is clearly seen to periodically vary in time. In a previous paper[47] we found that at the corresponding shear rates the director $\hat{\mathbf{n}}$ of the system being studied here performs kayaking motions. Here $\hat{\mathbf{n}}$ is the unit eigenvector of **S** corresponding to its largest eigenvalue, representing the average direction of the rods. Comparing viscosities and director motions, we find, to no surprise, that the peaks in the viscosities in panels a and b occur at strains where the directors flip from one flow aligned orientation to the other. Panel c corresponds to a shear rate just above the kayaking to wagging transition. Hence, the director is mainly situated in the shear plane, "wagging" about the velocity direction. The viscosity displays some small oscillations, which are rather insignificant compared to the absolute value. At very high shear rates, in panel d, the director is arrested in the shear plane, making a small angle with the flow direction. The corresponding viscosity is virtually constant.

In Figure 5 we display time-averaged viscosities as a function of shear rate, again for rods with aspect ratio $L/D = 25$, for

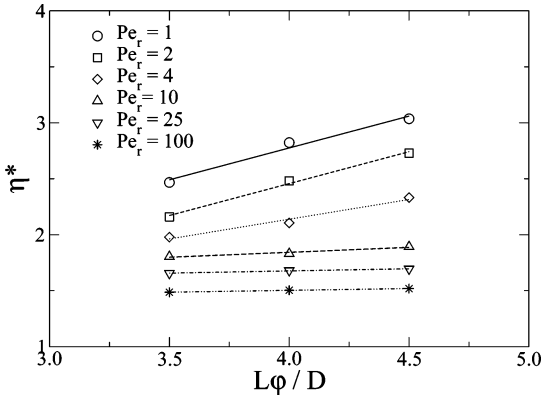

Figure 6. Relative viscosities of nematic solutions of rods with $L/D = 25$ as a function of the scaled volume fraction, for various shear rates ranging from $Pe_r = 1$ to 100.

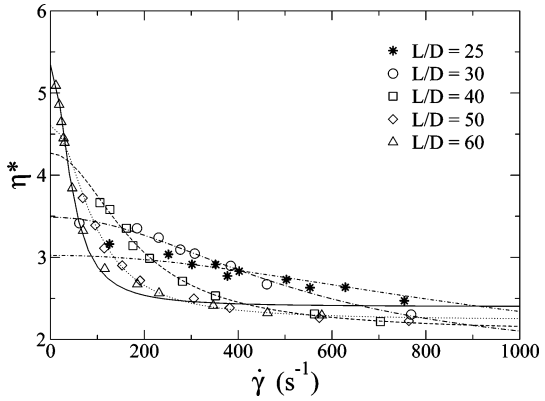

Figure 7. Relative viscosities of nematic systems as a function of shear rate. Solutions of rigid rods with $L/D = 25$ (stars), 30 (circles), 40 (diamonds), 50 (squares), and 60 (triangles) are investigated. The simulation results are fitted using the Hess formula[54] given in eq 12.

three different volume fractions. The drawn lines will be discussed later and should be considered as guides to the eye for the time being. As in the case of isotropic systems, a clear shear thinning is observed for all three volume fractions. In Figure 6 shear viscosities are shown to be linear in $L\varphi/D$ over a large range of shear rates.

Next, in Figure 7 we investigate the dependence of η^* on the aspect ratio L/D; the scaled volume fraction in all cases is given by $L\varphi/D = 4.5$. Two things may be noticed. First, the zero shear rate value of the viscosity increases substantially with increasing values of L/D. Second, the inflection point of the shear thinning curve moves to lower shear rates with increasing aspect ratios.

It is intuitively clear that the shear rate $\dot{\gamma}_{IP}$ at the inflection point of the viscosity curve reveals some dominant characteristic time in the system. It seems therefore to be appropriate to fit the shear thinning curves for nematic systems with the Hess equation, just as we did with the corresponding curves for isotropic systems. The drawn lines in Figures 5 and 7 were obtained in this way. Estimates of $\dot{\gamma}_{IP}$ are then calculated according to $\dot{\gamma}_{IP} = (\sqrt{3}\tau_r)^{-1}$. It is instructive to compare these values with the shear rates $\dot{\gamma}_{kw}$ at the kayaking to wagging transitions in the corresponding systems. Therefore, in Figure 8 we plot $\dot{\gamma}_{IP}/\dot{\gamma}_{kw}$ as a function of L/D for all systems studied in Figures 5 and 7. It is seen that for all aspect ratios $\dot{\gamma}_{IP}$ is almost equal to $\dot{\gamma}_{kw}$. The origin of shear thinning in nematic systems may therefore safely be attributed to the kayaking to wagging transition of the director.

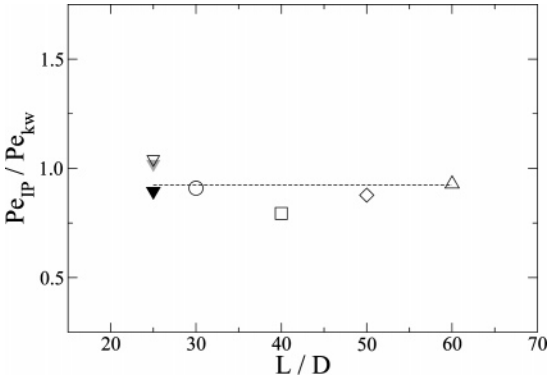

Figure 8. Ratio Pe_{kw}/Pe_{IP} as a function of aspect ratio. Pe_{kw} denotes the critical Peclet number at which the kayaking to wagging transition occurs, as obtained from inspection of the periodic orientational motions exhibited by the director. Pe_{IP} stands for the Peclet number calculated from the inflection point of the viscosity by using the Hess theory; see eq 12. Open symbols represent systems with a scaled volume fraction of 4.5, while the gray and solid triangles denote $L\varphi/D = 4.0$ and 3.5, respectively.

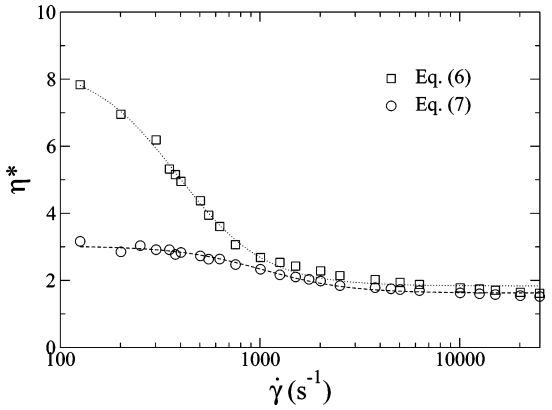

Figure 9. Comparison of the relative viscosities calculated by eq 6 (shown as squares) and eq 7 (circles) in nematic solutions of rods with $L/D = 25$ and $L\varphi/D = 4.5$ at various share rates. The dotted and dashed lines are fits by the Hess theory, eq 12.

Before finishing this subsection, let us make one more remark. In Figure 9 we have plotted flow curves, i.e., viscosities as a function of shear rate, for systems with $L/D = 25$ and $L\varphi/D = 4.5$, once calculated using eq 6 and once using eq 7. There is a clear difference between the two curves, with eq 6 producing the larger viscosities. On fitting the new curve with the Hess equation, we found that its inflection point occurs at a shear rate $\dot{\gamma}_{IP}$ which is a factor of 2.5 smaller than $\dot{\gamma}_{kw}$. This discrepancy may be considered a, be it weak, argument in favor of eq 7.

3.3. Normal Stress Difference. Measurements[28,29] of normal stress differences of nematic liquid crystalline polymers show remarkable differences compared with those exhibited by isotropic suspensions. For a concentrated yet isotropic solution, the first normal stress difference N_1 is always positive and increases monotonically with shear rate, while the second normal stress difference N_2 is negative and decreases with shear rate. In nematic solutions, on the other hand, highly nonlinear rheological behaviors are observed: both the first and the second normal stress differences change signs several times with increasing shear rate.

In Figure 10, we plot N_1 and $-N_2$ as a function of the rotational Peclet number in a log−log scale. The scaled volume fraction $L\varphi/D$ is chosen equal to 2.0, ensuring an isotropic system.[46] The monotonic increase in magnitude of both N_1 and N_2 agrees qualitatively with experimental results on rodlike

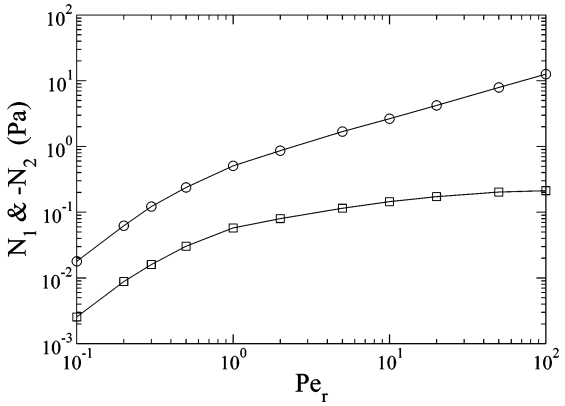

Figure 10. First (shown as circles) and second (squares; note the reversal of sign) normal stress differences of isotropic solutions of rigid rods with $L/D = 25$ as a function of rotational Peclet number. The scaled volume fraction $L\varphi/D$ is chosen equal to 2.0.

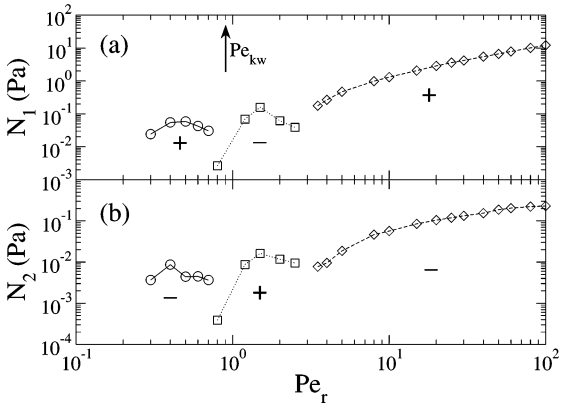

Figure 11. Absolute values of the first and second normal stress differences of nematic solutions of rigid rods with $L/D = 25$ and $L\varphi/D = 3.5$ as a function of rotational Peclet number are plotted in (a) and (b) in the log−log scale, respectively. The critical Peclet number of the kayaking to wagging transition, Pe_{kw}, is represented by an arrow.

PBLG (poly(γ-benzyl L-glutamate)) in the isotropic phase by Magda et al.[32] It is well-known that the probability distribution function of the end-to-end vector of polymers, whether flexible or rigid, in isotropic phases is distorted from spherical to ellipsoidal distributions when such systems are subjected to shear flow. The resulting elastic forces must be balanced by shear forces, making Σ_{xx} invariably positive and Σ_{yy} negative.[9] Since the flow hardly influences the distribution in the vorticity direction, Σ_{zz} remains very small, and the normal stress differences have the signs found in our simulation.

The absolute values of N_1 and N_2 of nematic suspensions are plotted as a function of Peclet number in parts a and b of Figure 11, respectively. The aspect ratio L/D is chosen equal to 25 again, while the scaled volume fraction $L\varphi/D = 3.5$, ensuring the nematic state of the systems. Compared with the behaviors shown by the isotropic suspensions, distinctive phenomena are observed in nematic phases: both normal stress differences are not monotonic anymore but change sign with shear rate. The first normal stress difference N_1 is found positive at low and high shear rates but negative at intermediate shear rates. The second normal stress difference N_2 is much smaller in magnitude than N_1 and always opposite in sign. This feature of N_2 is in accordance with that shown by isotropic solutions.

As can be read from Figure 11, the first change of sign occurs exactly at the transition from kayaking to wagging, indicated by an arrow at the upper horizontal axis, while the second change of sign occurs around the transition from wagging to

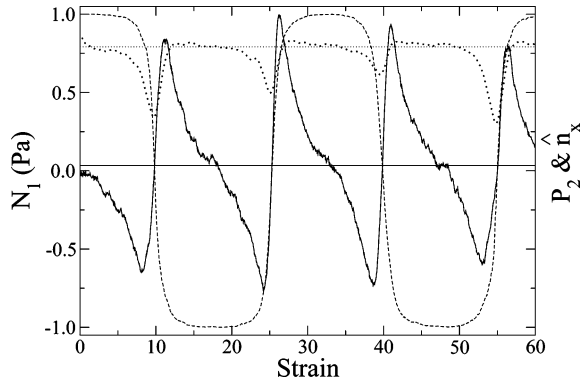

Figure 12. First normal stress difference N_1 (drawn curve), the scalar order parameter P_2 (dotted), and the x component of the director (dashed) of the nematic solution of rods with $L/D = 25$ and $L\varphi/D = 3.5$ as a function of strain. The upper and lower horizontal lines represent the equilibrium scalar order parameter and the time average of the first normal stress difference, respectively. At the applied shear rate $\dot{\gamma} = 125\ s^{-1}$, the director exhibits a tumbling/kayaking motion.

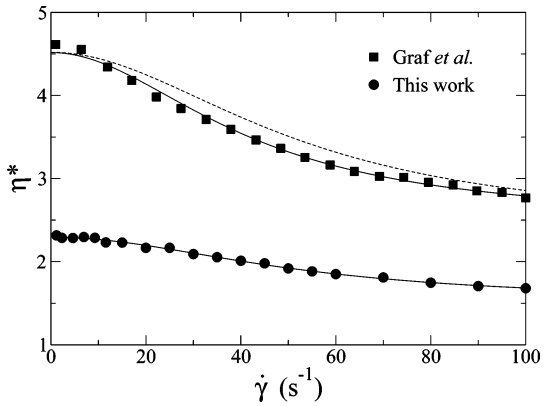

Figure 13. Relative viscosities of solutions of *fd* viruses (squares: experimental[36] with 1.56 mg/ml *fd* in 100 mM NaCl; circles: simulations with $L/D = 60$ and $L\varphi/D = 0.5$) as a function of shear rate. Solid curves are fits using the Hess theory eq 12 on the basis of experimental and simulation data. The dashed curve denotes the simulated viscosities following a rescaling by $1 + [(\eta^*_{exp}(0) - 1)/(\eta^*_{sim}(0) - 1)](\eta^*_{sim}(\dot{\gamma}) - 1)$; see text for details.

flow-aligning, which is difficult to pinpoint otherwise. This complex behavior was first analyzed by Marrucci and Maffettone[9] on the basis of the two-dimensional analogue of the Doi−Hess theory. A three-dimensional analysis was provided by Larson,[12] who found three distinct regions very much in agreement with our results. The elastic response of the flow aligned state is to a large extent similar to that of the isotropic state. The orientational probability distribution is already rather narrow at zero shear, since we are in a nematic state. The flow has aligned this distribution along the flow direction and tries to narrow it just like in the isotropic state. The system is therefore rather similar to that in the isotropic state explaining the signs of N_1 and N_2.

In Figure 12 we have plotted the first normal stress difference N_1, the scalar order parameter P_2, and the x component of the director $\hat{n}_x$ of a tumbling system with $L/D = 25$, $L\varphi/D = 3.5$, and $\dot{\gamma} = 125\ s^{-1}$ as a function of strain. N_1 has been calculated on the basis of eq 7, including the term proportional to d**S**/dt. We find that N_1 is basically equal to Σ_{xx}. From the plot we see that N_1 rises sharply every time when the rods tumble. After the rods have settled along the flow direction, P_2 is somewhat larger than its equilibrium value at the given value of $L\varphi/D$. N_1, and so also Σ_{xx}, begin to gradually decrease and become negative when P_2 drops below its equilibrium value. At this stage Σ_{xx} opposes the elastic forces caused by the fact that the orientational distribution is too wide for the given value of $L\varphi/D$. N_1 continues to decrease until the whole process starts again with the next tumbling.

As a final remark we notice that the normal stress differences N_1 and N_2 calculated by eq 6 are monotonic against shear rate. Since this is not in agreement with experimental observation, we once more conclude that eq 7 provides a much safer expression to calculate stresses than eq 6.

4. Conclusions

We have calculated relative viscosities as well as first and second normal stress differences of suspensions of rigid liquid crystalline polymers in shear flow. To make this goal realizable, a recently developed event-driven Brownian dynamics algorithm was used. In this algorithm, excluded-volume interactions between the rods are considered to be infinitely hard, but hydrodynamic interactions are neglected.

The general picture of the present paper is summarized as follows:

1. The suspensions of rigid rods exhibit shear thinning behavior in shear flow, both in isotropic and in nematic states.

2. In the isotropic phase, the measured shear thinning curves accord very well with the Hess equation. At low volume fractions or low shear rates, results by Dhont and Briels were confirmed. The self-rotational diffusion coefficients calculated by fitting the simulation results with the Hess equation show good agreement with traditional measurements.

3. The inflection points of the shear thinning curves of nematic systems are associated with the shear rates at which the director transforms its orientational motion from kayaking to wagging. Our calculated values of the inflection points are in good agreement with those measured by investigating the motion of the director.

4. The first normal stress difference N_1 in nematic solutions of rigid rods is positive at low or high shear rates but negative when intermediate shear rates are employed. The second normal stress difference N_2 is found always with opposite sign to that of N_1 and much smaller in amplitude. These fascinating behaviors are rather distinguished compared to the monotonic properties that are exhibited by isotropic solutions. Our simulation results qualitatively confirm both theoretical predictions and experimental measurements.

It is constructive to make a quantitative comparison between our simulations and experiments on rodlike polymers. In Figure 13, we have plotted the experimental viscosities of isotropic solutions of *fd* viruses measured by Graf et al.[36] Using a molar weight[49] of 1.64×10^7 g/mol and an effective aspect ratio of 60, the experimental density of 1.56 mg/ml corresponds to a scaled volume fraction of 0.5. Simulated viscosities of rod suspensions with $L/D = 60$ and $L\varphi/D = 0.5$ are shown as circles. The simulations deviate from the experiments by a factor of 2. Considering the inherent flexibility of the *fd* virus and the ionic strength in the aqueous solution, which highly affects the effective diameter of the virus, this discrepancy is reasonable. Scaling the contribution of the rods such that the simulated and experimental viscosities agree at zero shear rate makes them agree at all shear rates. This scaling roughly amounts to multiplying $\eta^*_{sim}(\dot{\gamma}) - 1$, and hence $\alpha\ L\varphi/D$, by a factor of $(\eta^*_{exp}(0) - 1)/(\eta^*_{sim}(0) - 1)$.

Acknowledgment. This work is part of the SoftLink research program of the Stichting voor Fundamenteel Onderzoek der

CDV

Materie (FOM), which is financially supported by the Nederlandse Organisatie voor Wetenschappelijk Onderzoek (NWO). We thank Prof. Jan K. G. Dhont for many useful discussions.

References and Notes

(1) Hess, S. *Z. Naturforsch. A* **1976**, *31*, 1034.
(2) Doi, M. *J. Polym. Sci., Polym. Phys. Ed.* **1981**, *19*, 229.
(3) Jain, S.; Cohen, C. *Macromolecules* **1981**, *14*, 759.
(4) Fesciyan, S.; Dahler, J. S. *Macromolecules* **1982**, *15*, 517.
(5) Dahler, J. S.; Fesciyan, S.; Xystris, N. *Macromolecules* **1983**, *16*, 1673.
(6) Altenberger, A. R.; Dahler, J. S. *Macromolecules* **1985**, *18*, 1700.
(7) Doi, M.; Edwards, S. F. *The Theory of Polymer Dynamics*; Clarendon: Oxford, 1986.
(8) Davis, R. M.; Russel, W. B. *Macromolecules* **1987**, *20*, 518.
(9) Marrucci, G.; Maffettone, P. L. *Macromolecules* **1989**, *22*, 4076.
(10) Marrucci, G.; Maffettone, P. L. *J. Rheol.* **1990**, *34*, 1217.
(11) Marrucci, G.; Maffettone, P. L. *J. Rheol.* **1990**, *34*, 1231.
(12) Larson, R. G. *Macromolecules* **1990**, *23*, 3983.
(13) Marrucci, G. *Macromolecules* **1991**, *24*, 4176.
(14) Larson, R. G.; Doi, M. *J. Rheol.* **1991**, *35*, 539.
(15) Larson, R. G.; Öttinger, H. C. *Macromolecules* **1991**, *24*, 6270.
(16) Larson, R. G. *Rheol. Acta* **1992**, *31*, 213.
(17) Larson, R. G. *The Structure and Rheology of Complex Fluids*; Oxford University Press: New York, 1999.
(18) Faraoni, V.; Grosso, M.; Crescitelli, S.; Maffettone, P. L. *J. Rheol.* **1999**, *43*, 829.
(19) Dhont, J. K. G.; Briels, W. J. *J. Chem. Phys.* **2002**, *117*, 3992.
(20) Dhont, J. K. G.; Briels, W. J. *Colloids Surf., A* **2003**, *213*, 131.
(21) Dhont, J. K. G.; Briels, W. J. *J. Chem. Phys.* **2003**, *118*, 1466.
(22) Hess, S.; Kröger, M. *J. Phys.: Condens. Matter* **2004**, *16*, S3858.
(23) Forest, M. G.; Wang, Q. *J. Non-Newtonian Fluid Mech.* **1999**, *83*, 131.
(24) Forest, M. G.; Zhou, R.; Wang, Q. *J. Rheol.* **2003**, *47*, 105.
(25) Forest, M. G.; Wang, Q.; Zhou, R. *Rheol. Acta.* **2004**, *44*, 80.
(26) Zheng, X.; Forest, M. G.; Zhou, R.; Wang, Q. *Rheol. Acta.* **2005**, *44*, 219.
(27) Siettos, C.; Graham, M. D.; Kevrekidis, I. G. *J. Chem. Phys.* **2003**, *118*, 10149.
(28) Kiss, G.; Porter, R. S. *J. Polym. Sci., Polym. Symp.* **1978**, *65*, 193.
(29) Kiss, G.; Porter, R. S. *J. Polym. Sci., Polym. Phys. Ed.* **1978**, *18*, 361.
(30) Moldenaers, P.; Fuller, G.; Mewis, J. *Macromolecules* **1989**, *22*, 960.
(31) Burghardt, W. R.; Fuller, G. G. *Macromolecules* **1991**, *24*, 2546.
(32) Magda, J. J.; Baek, S.-G.; DeVries, K. L.; Larson, R. G. *Macromolecules* **1991**, *24*, 4460.
(33) Chow, A. W.; Harlin, R. D.; Ylitalo, C. M. *Macromolecules* **1992**, *25*, 7135.
(34) Hongladarom, K.; Burghardt, W. R.; Baek, S.-G.; Cementwala, S.; Magda, J. J. *Macromolecules* **1993**, *26*, 772.
(35) Hongladarom, K.; Burghardt, W. R. *Macromolecules* **1993**, *26*, 785.
(36) Graf, C.; Kramer, H.; Deggelmann, M.; Hagenbüchle, M.; Johner, C.; Weber, R. *J. Chem. Phys.* **1993**, *98*, 4920.
(37) Baek, S.-G.; Magda, J. J.; Larson, R. G. *J. Rheol.* **1993**, *37*, 1201.
(38) Baek, S.-G.; Magda, J. J.; Larson, R. G.; Hudson, S. D. *J. Rheol.* **1994**, *38*, 1473.
(39) Zirnsak, M. Z.; Hur, D. U.; Boger, D. V. *J. Non-Newtonian Fluid Mech.* **1994**, *54*, 153.
(40) Mewis, J.; Mortier, M.; Vermant, J.; Moldenaers, P. *Macromolecules* **1997**, *30*, 1323.
(41) Lettinga, M. P.; Dogic, Z.; Wang, H.; Vermant, J. *Langmuir* **2005**, *21*, 8048.
(42) Yamane, Y.; Kaneda, Y.; Doi, M. *J. Non-Newtonian Fluid Mech.* **1994**, *54*, 405.
(43) Yamane, Y.; Kaneda, Y.; Doi, M. *J. Phys. Soc. Jpn.* **1995**, *64*, 3265.
(44) Mori, N.; Fujioka, H.; Semura, R.; Nakamura, K. *Rheol. Acta* **2003**, *42*, 102.
(45) Tao, Y.-G.; den Otter, W. K.; Briels, W. J. *Phys. Rev. Lett.* **2005**, *95*, 237802.
(46) Tao, Y.-G.; den Otter, W. K.; Dhont, J. K. G.; Briels, W. J. *J. Chem. Phys.* **2006**, *124*, 134906.
(47) Tao, Y.-G.; den Otter, W. K.; Briels, W. J. *J. Chem. Phys.* **2006**, *124*, 204902.
(48) Tao, Y.-G.; den Otter, W. K.; Padding, J. T.; Dhont, J. K. G.; Briels, W. J. *J. Chem. Phys.* **2005**, *122*, 244903.
(49) Lenstra, T. A.; Dogic, Z.; Dhont, J. K. G. *J. Chem. Phys.* **2001**, *114*, 10151.
(50) Dogic, Z.; Fraden, S. *Philos. Trans. R. Soc. London A* **2001**, *359*, 997.
(51) Dogic, Z.; Fraden, S. *Curr. Opin. Colloid Interface Sci.* **2006**, *11*, 47.
(52) Allen, M. P.; Tildesley, D. J. *Computer Simulation of Liquids*; Clarendon: Oxford, 1987.
(53) Hess, S. *Physica A* **1977**, *87*, 273.
(54) Hess, S. *Z. Naturforsch. A* **1980**, *35*, 915.
(55) Maguire, J. F.; McTague, J. P. *Phys. Rev. Lett.* **1980**, *45*, 1891.
(56) Nakamura, H.; Okano, K. *Phys. Rev. Lett.* **1983**, *50*, 186.
(57) Kramer, H.; Deggelmann, M.; Graf, C.; Hagenbüchle, M.; Johner, C.; Weber, R. *Macromolecules* **1992**, *25*, 4325.

MA060622Q